Mechanisms of Buoyancy Transport through Mixed Layers and Statistical Signatures from Isobaric Floats

CHRISTOPHE HERBAUT

Laboratoire d'Oceanographie Dynamique et de Climatologie, Paris, France

JOHN MARSHALL

Department of Earth, Atmospheric and Planetary Sciences, Massachusetts Institute of Technology, Cambridge, Massachusetts

(Manuscript received 12 June 2000, in final form 11 June 2001)

ABSTRACT

Idealized nonhydrostatic numerical calculations that resolve both plumes and geostrophic eddies are used to mimic isobaric float observations taken in the Labrador Sea Deep Convection Experiment and study mechanisms of buoyancy transport through mixed layers. The plumes and eddies are generated in a periodic channel, initialized with a vertical profile of temperature, and cooled by surface heat loss varying across the channel. Probability density functions and time series of vertical velocity and temperature computed from the floats are interpreted in terms of the kinematics of plumes and geostrophic eddies, and their role in buoyancy transport. Estimates from Eulerian time series from the numerical model suggest that geostrophic eddies and plumes have a comparable contribution to vertical heat flux.

1. Introduction

A central objective of the Labrador Sea Deep Convection Experiment was to observe and understand the mechanisms of buoyancy transport through a deepening mixed layer. The process is complicated because it conjoins two distinct physical processes—upright/slantwise convection and baroclinic instability (see Haine and Marshall 1998, hereafter HM)—which together transport buoyancy through the mixed layer. In the deep convection regime these processes occur together on scales at which the hydrostatic approximation is breaking down (for a review see Marshall and Schott 1999). A description of the buoyancy and vertical velocity fluctuations that accomplish the lateral and vertical transport of buoyancy is needed. A three-dimensional mapping of these fields, spanning scales from a few meters out to several kilometers, would be desirable but not yet achievable. A more practical goal is a description of the statistics of these fields. During the experiment isobaric floats designed to observe the vertical circulation and buoyancy fluctuations associated with them were deployed (see Lavender et al. 2002), and statistical signatures of the vertical velocity, w, and temperature fields, T, were obtained. These observations, briefly reviewed in section 2, motivate the present study.

In section 3, idealized nonhydrostatic numerical calculations are described that resolve both plumes and geostrophic eddies, mimicking the float observations taken in the field. Statistical signatures following isobaric floats are compared to Eulerian statistics. In section 4, simple scaling laws are derived, supported by our numerical experiments, that relate the lateral buoyancy transport due to baroclinic eddies to the strength of the horizontal currents set up by the buoyancy forcing of the fluid. In section 5 we summarize and conclude.

2. Plumes versus eddies

a. Observations of plumes and eddies from autonomous floats

Float deployment in convective regions is rare. Stommel et al. (1971) were the first to measure strong vertical velocity ($\sim$10 cm s^{-1} in the Western Mediterranean). Gascard and Clarke (1983) deployed three floats with vertical current meters (VCMs) in the Labrador Sea Water formation region. The float measurements described mesoscale activity (deduced from the float trajectories) and plume activity characterized by strong vertical velocity (maximum downward velocity observed by the float was 9 cm s^{-1}). The most recent measurements were done during the Labrador Sea Deep Convection Experiment (see Lab Sea Group 1998). There, field work was embedded within an array of autonomous floats

Corresponding author address: Dr. John Marshall, Dept. of Earth, Atmospheric and Planetary Sciences, Massachusetts Institute of Technology, Room 54-1526, Cambridge, MA 02139-4307.
E-mail: marshall@gulf.mit.edu

deployed as part of the World Ocean Circulation Experiment (WOCE) Atlantic Circulation and Climate Experiment (ACCE). The floats were programmed to move at a depth of either 1500 or 400 m and periodically profile the *T* and *S* of the column. As described in Lavender et al. (2002), the floats observed the creation of a deep convecting layer involving both vertical exchange and lateral interleaving of water masses. It appears that convection reached about 1200 m by the end of March 1997. But the convection layer was far from uniform, neither vertically nor horizontally. A great deal of variability in temperature and salinity profiles was observed from the lateral interleaving of waters of different *T* and *S* but similar densities. These inhomogeneities arise because of variability in the preexisting temperature and salinity fields (see Legg and McWilliams 2000), but also because the buoyancy flux through the sea surface varies strongly in space (as well as time), decaying rapidly from the western boundary [see Fig. 11 of Lab Sea Group (1998), which reveals variations of heat flux of 500–600 W m^{-2} over a distance of 200 km or so].

In the winters of 1996/97 and 1997/98 (hereafter 1997 and 1998), autonomous floats, similar to those deployed in ACCE but equipped with VCMs, were deployed in the western Labrador Sea where deep convection was expected to be most vigorous (see Lab Sea Group 1998). The VCM floats were programmed to profile temperature and salinity to 1600 m every 5 days and to record 4-day time series of temperature and vertical velocity from a depth near 400 m while following horizontal flow. Most of the VCM floats encountered deep mixed layers as indicated by evolution of their *T* and *S* profiles. They observed strong but chaotic motion at 400 m with 4-day average horizontal velocities of 10–20 cm s^{-1} quite common, substantially stronger flows than obtained from the deeper floats. The VCMs recorded vigorous vertical velocities associated with convection. Vertical flows of 5 cm s^{-1} were frequent, and there is one example of a plume with peak downward speeds of 10 cm s^{-1} and a duration of 6–8 h. The event duration is much longer than was seen in the moored results, consistent with the idea that plumes with widths of order 500 m were advected by the moorings, while the VCM approximately follows the plume's horizontal motion.

b. PDFs of w

Figure 1 shows the probability density function (PDF) of the w' observed by the VCMs deployed during the experiment for winter 1997 and 1998 at a depth of ~400 m. A detailed description of these statistics can be found in Lavender et al. (2002). Here we note that *w* lie in the range ± 10 cm s^{-1} and are rather symmetric about the origin. There is a skewness in the *w* PDF, however, which is largest during the period of highest fluxes—the floats experience more downward *w* than upward.

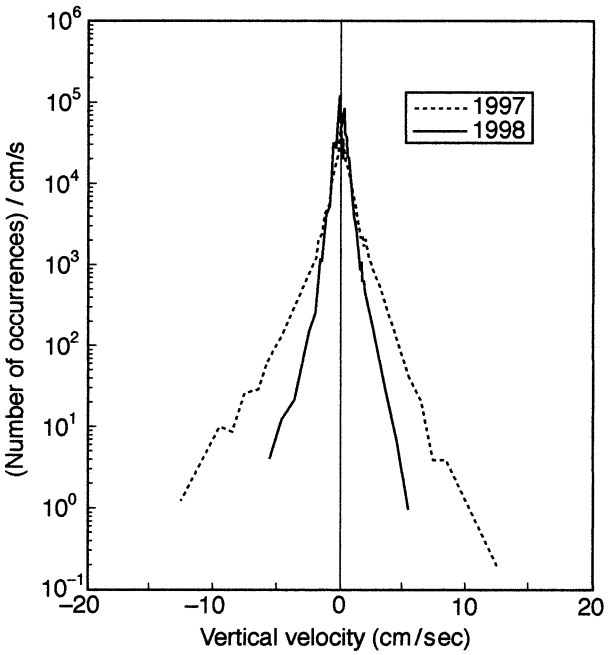

FIG. 1. Probability density function of the vertical velocity measured by Profiling Autonomous Langrangian Circulation Explorer (PALACE) floats deployed in the Lab Sea Expt (see Lab Sea Group 1998; Lavender et al. (2002) during 1997 and 1998.

As discussed below, if floats sample a field of convective plumes at upper levels where dense fluid converges into plumes, then one might expect them to experience downwelling more often than upwelling, leading to a skewness of the PDFs. However, if VCMs experience a field of geostrophic turbulence energized by the convective process, with strong variations of the mixed layer depth, then their PDFs may not be strongly skewed. We will also see that the geostrophic scales can efficiently transport buoyancy both horizontally and vertically without a pronounced skewness in the PDF of *w* more typical of plumes.

3. Numerical studies

a. Reference calculation

In order to explore the mechanisms of buoyancy transport through mixed layers by plumes and eddies we employ the model described in Marshall et al. (1997a,b), which solves the nonhydrostatic equations for a Boussinesq fluid using finite-volume techniques. Our purpose here is not to simulate the details of convection observed in the Labrador Sea experiment, but rather to set up idealized experiments in which the controlling dynamics can be studied and the statistical signatures that reveal them explored.

The setup of the numerical experiments follows that of HM, to which the reader is referred for more detail. Briefly, a periodic channel with constant depth of 2000 m is used of, nominally, length 60 km and width 20

km. The cell dimension is 250 m in the horizontal, with vertical spacing varying between 40 m at the surface and 400 m at the bottom. To represent unresolved dynamics and ensure numerical stability, a Laplacian diffusion of heat and momentum is applied. The diffusivities and viscosities are set equal with horizontal and vertical magnitudes of 5 and 0.02 $m^2\ s^{-1}$, respectively. The time step is 60 s. Free slip is allowed at the solid boundaries.

The channel contains an initially motionless fluid of stratification N_{th}^2 in the presence of rotation, f. A spatially varying buoyancy forcing is then applied at its upper surface. We choose to begin our calculations from rest so that we can study the transition from upright convection to baroclinic instability and the concomitant change in statistical signatures measured by floats. We specify a linearized equation of state with one thermodynamically active variable:

$$\rho = \rho_0[1 - \alpha(T - T_0)],$$

where the expansion coefficient α is $2 \times 10^{-4}\ K^{-1}$ at temperature T_0. At the sea surface a buoyancy flux is prescribed that varies across the channel according to a hyperbolic tangent, thus:

$$B = B_{1/2}\left[\tanh\left(2\frac{(y - L_y/2)}{L_f}\right) + 1\right], \qquad (1)$$

where $B_{1/2}$ is the buoyancy flux at midchannel, y is the distance across the channel, L_y is the channel width, and L_f is a characteristic length scale of the forcing. The tanh function smoothly increases the forcing from zero on the southern boundary to a maximum of $2B_{1/2}$ at the northern boundary and provides a well-defined maximum gradient in flux, located at the channel center. This allows a mixed layer to grow that is deeper on one side of the channel than the other, inducing a lateral density gradient and a thermal wind in balance with it. The spatial gradients imposed by (1) are strong with respect to the gradients in buoyancy forcing induced by the prevailing meteorology, which decays rapidly away from the western boundary of the Labrador Sea.

Parameters of the experiments studied here are set out in Table 1.

TABLE 1. Key parameters of the numerical experiments. A channel of length 60 km and width 20 km was used in all calculations.

Expt	N_{th} (10^{-4} s^{-1})	f (10^{-4} s^{-1})	L_f (km)	H (W m^{-2})	$B^{1/2}$ (10^{-7} $m^2\ s^{-3}$)	l_{rot} (m)
1	2.24	1.0	10	400	1.96	443
2	8.37	1.0	10	400	1.96	443
3	16.7	1.0	10	400	1.96	443
4	8.37	1.0	10	100	0.49	221
5	4.18	1.0	10	400	1.96	443
6	8.37	1.0	10	800	3.92	626
7	8.37	1.0	10	50	0.24	157
8	8.37	0.5	10	200	0.98	886
9	8.37	2.0	10	200	0.98	111

THE TRANSITION FROM CONVECTION TO BAROCLINIC EDDIES

In this section we will discuss the results of the second experiment (expt 2). A typical example of the flow development is shown in Fig. 2. The near-surface fields of w reveal progression from plume-scale convection at day 2 confined to the northern half of the channel, where the cooling is the strongest. By day 5, the plumes are being organized by the developing larger-scale geostrophic flow until, by day 9, strong downwelling regions are confined almost entirely to frontal regions (see Fig. 2, bottom). Here downwelling in excess of 10 cm s^{-1} can be sustained. Weaker upwelling regions occur on the large scale but also in regions adjacent to the northern boundary. A similar behavior is observed in numerical studies of the localization of deep convection by a mesoscale eddy (see Legg et al. 1998). There an initial geostrophically balanced eddy is broken apart by baroclinic instability with downward motion being concentrated in the thermal front that separates the interior of the eddy from its exterior (see Fig. 3a of Legg et al. 1998).

A surface-intensified zonal jet evolves in balance with the across-channel temperature gradient (the temperature field is contoured in Fig. 2), with the eddying part of the flow dominating. Since there is no stress applied at the surface, the global zonal momentum cannot change, and eastward flow at the surface is compensated, by a westward current below. The length scale for the baroclinic instability at day 9 is around 10 km. This scale can be understood in terms of baroclinic instability theory, as discussed in HM.

Figures 3a and 3c show the zonal mean sections of temperature at days 5 and 9, respectively. By day 5 the one-dimensional, vertical convection that dominates the convective layer in the initial stages has generated a mixed patch of fluid adjacent to the northern wall of the channel, except near the surface where static instability prevails due to surface cooling. But by day 9 it is unclear how to distinguish between mixed layer fluid and the underlying water based on the temperature field alone. The convectively active layer is not mixed in buoyancy—baroclinic eddies act to restratify the layer, drawing buoyant fluid from the south to seal over the surface layer.

We believe that symmetric instability is also an important player in the evolution of the downwelling fronts. This mechanism was discussed in an axisymmetric context, in HM, in which zonal absolute momentum is conserved (see also Marshall and Schott 1999). Figure 3b shows temperature (shaded), absolute momentum ($u - fy$; contoured), and velocity (vectors) in the meridional plane cutting through the downwelling front located at $x = 47.5$ km in Fig. 2c. We see upright convection in the north of the section. But to the south,

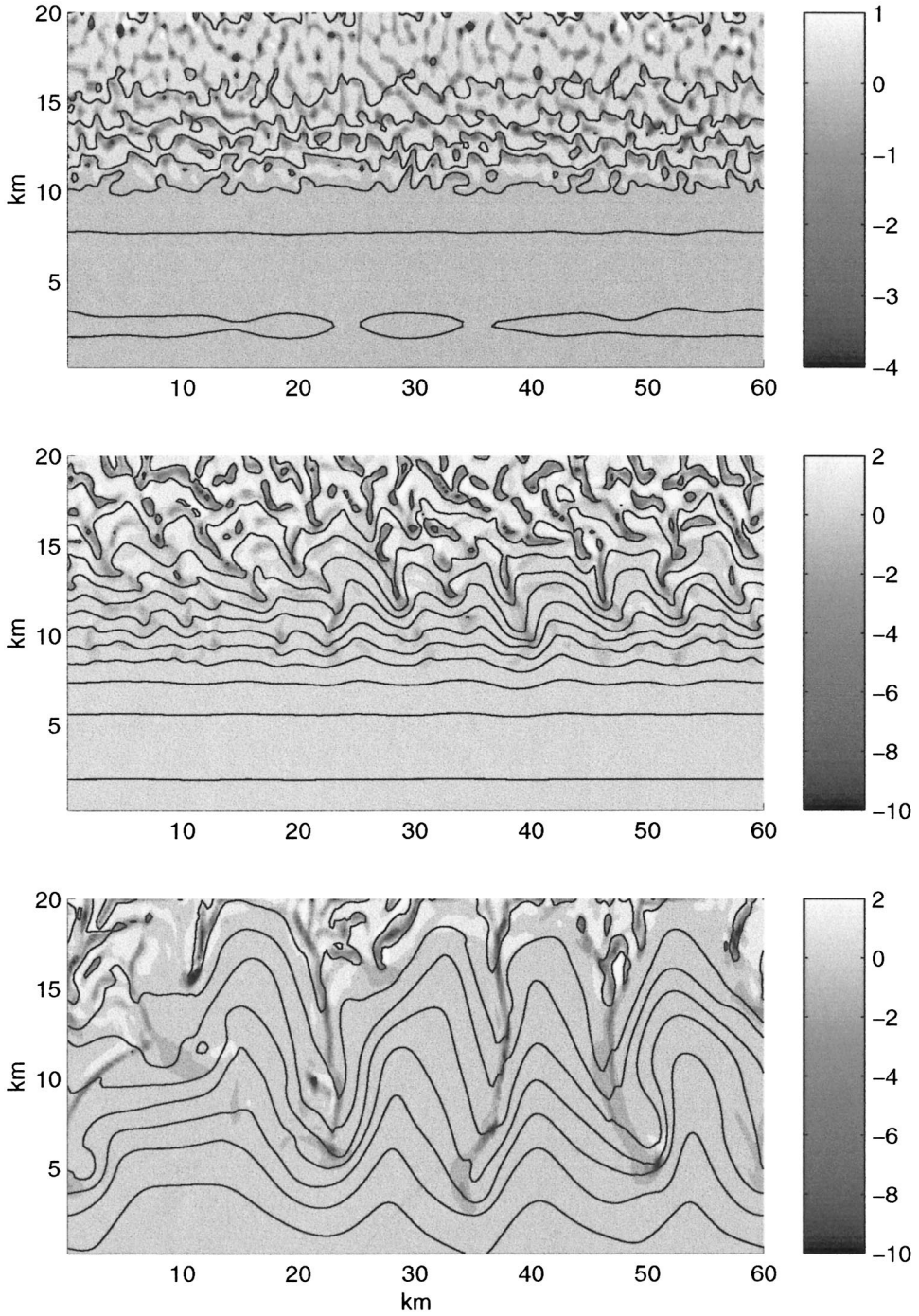

FIG. 2. Vertical velocity (cm s^{-1}) in gray and temperature (solid lines) at a depth of 300 m from expt 2 (top) at day 2, (middle) at day 5, and (bottom) at day 9 (contour interval of 0.05°C for temperature).

frontal downwelling is slanted along the absolute momentum surfaces. Slantwise convection was also observed in the numerical study of Legg et al. (1998). There symmetric instability develops before the onset of baroclinic instability and participates in the restratification of the interior of the eddy. In the present study the two processes coexist and cannot be so clearly separated from one another.

Figure 4 shows plots analogous to Fig. 2 but in the case where the imposed buoyancy loss has no spatial gradients. A homogeneous field of plumes emerges that uniformly fills space. No large-scale flow develops,

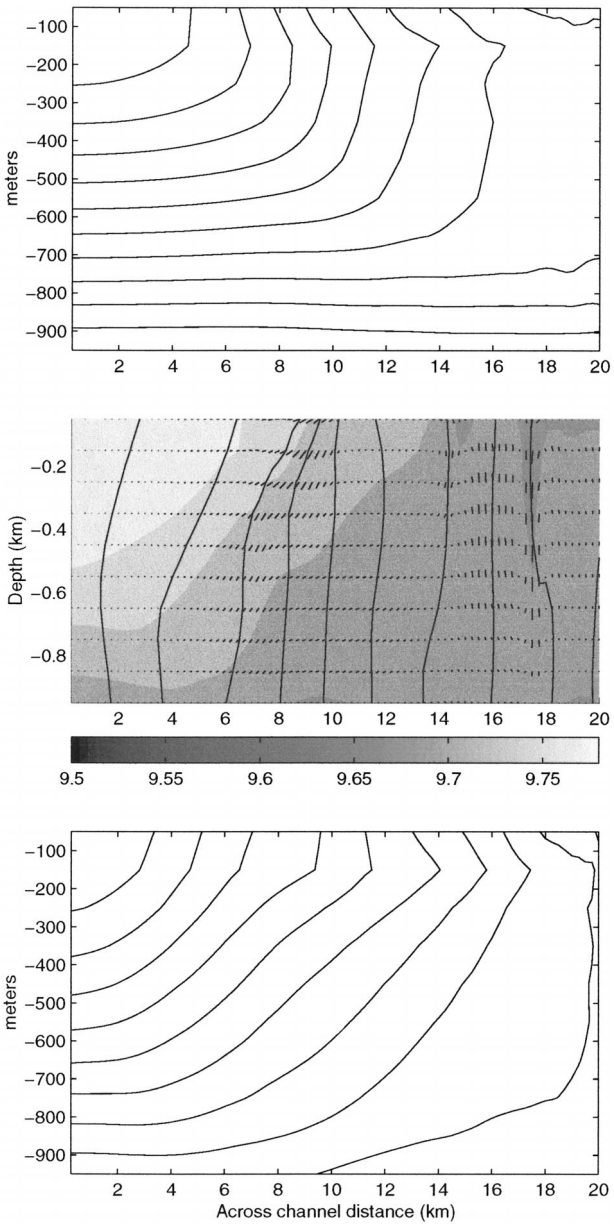

FIG. 3. Across-channel section of zonal mean temperature (top) at day 5 (contour interval 0.02°C) in expt 2. Across-channel section of temperature at $x = 47.5$ km (grayscale change every 0.02°C) (middle) at day 9. Absolute momentum surfaces (solid lines, contour interval of 0.2 m s^{-1}) and the flow (vectors) are also shown. Across-channel section of zonal mean temperature (bottom) at day 9 (contour interval 0.02°C).

plumes and geostrophic scales do not coexist, and no frontal regions with strong downward motions appear.

b. Statistical signatures of plumes and eddies

The evolving numerical fluid was seeded with floats in two experiments with different initial stratifications. In the first (expt 1), for which the stratification is weak ($N^2_{\text{th}} = 5 \times 10^{-8}$ s^{-2}), the model was seeded with 90 isobaric floats, roughly the number deployed in the field. At the initial time, the floats were regularly positioned every 6 km at three levels (300, 800, and 1500 m) to sample the upper, middle, and lower regions of the convection layer. Temperature and vertical velocity are stored every 10 minutes along the float tracks, just as for the floats in the field. The float trajectories were computed using a fourth-order Runge–Kutta method, with a 60-s time step using linear interpolation.

Figure 5 displays the trajectories of two floats located at, respectively, 300 and 800 m. During the first five days the floats do not drift far from their initial position, and their trajectories are dominated by small-scale motions induced by plumes. Beyond five days the trajectories show larger loops responding to the buildup of advection by mesoscale motions.

Inspection of the float record in Fig. 5 reveals events of 3–6 h duration associated with large downward vertical velocities characteristic of plumelike behavior. However, the time series of temperature is quite decorrelated with that of *w*: variations in temperature are typically associated with longer timescales and mesoscale motions (loops in the trajectories) that sweep the float to and from vertically mixed and stratified regions of the flow. A general downward trend, due to cooling, is also evident. An example of the decorrelation between *T* and *w* can be seen in Fig. 5a: at day 5.4 a strong downward motion does not produce any significant variation in temperature, while a vigorous plume event at day 6 appears to be associated with a small decrease in temperature. This decorrelation between *w* and *T* is also a characteristic of real float data; Figs. 4a and 4b are very similar to Figs. 14b and 14c of Lavender et al. (2002), but note that in our model, and unlike in the ocean, density is only a function of temperature, so comparisons with real data must be carried out with care. In regions where we can suppose that the stratification is weak [the temperature varies from 2.72° to 2.76°C in Fig. 14b of Lavender et al. (2002)], the floats see large upward and downward vertical motions and only tiny temperature variations. These authors suggest that the low correlation between *w* and *T* cannot be due to internal waves. It is likely that, as in our numerical experiment, they are a consequence of the lateral advection of the float by large-scale motions that carry the float into regions of very different vertical stratification.

The PDFs of the vertical velocities computed at the float positions show a strong initial asymmetry that reduces as time proceeds (see Fig. 6). These PDFs are computed by calculating the frequency of occurrence of vertical velocity over 1-day periods. The PDF of the vertical velocity at 300 m, fig. 6a, is skewed, with downward vertical velocities occurring more frequently than upward vertical velocities for days 2 and 3 (red line). As time proceeds the asymmetry is reduced. The PDFs of *w* at 800 m, fig. 6b, show an opposite asymmetry that becomes less marked with time.

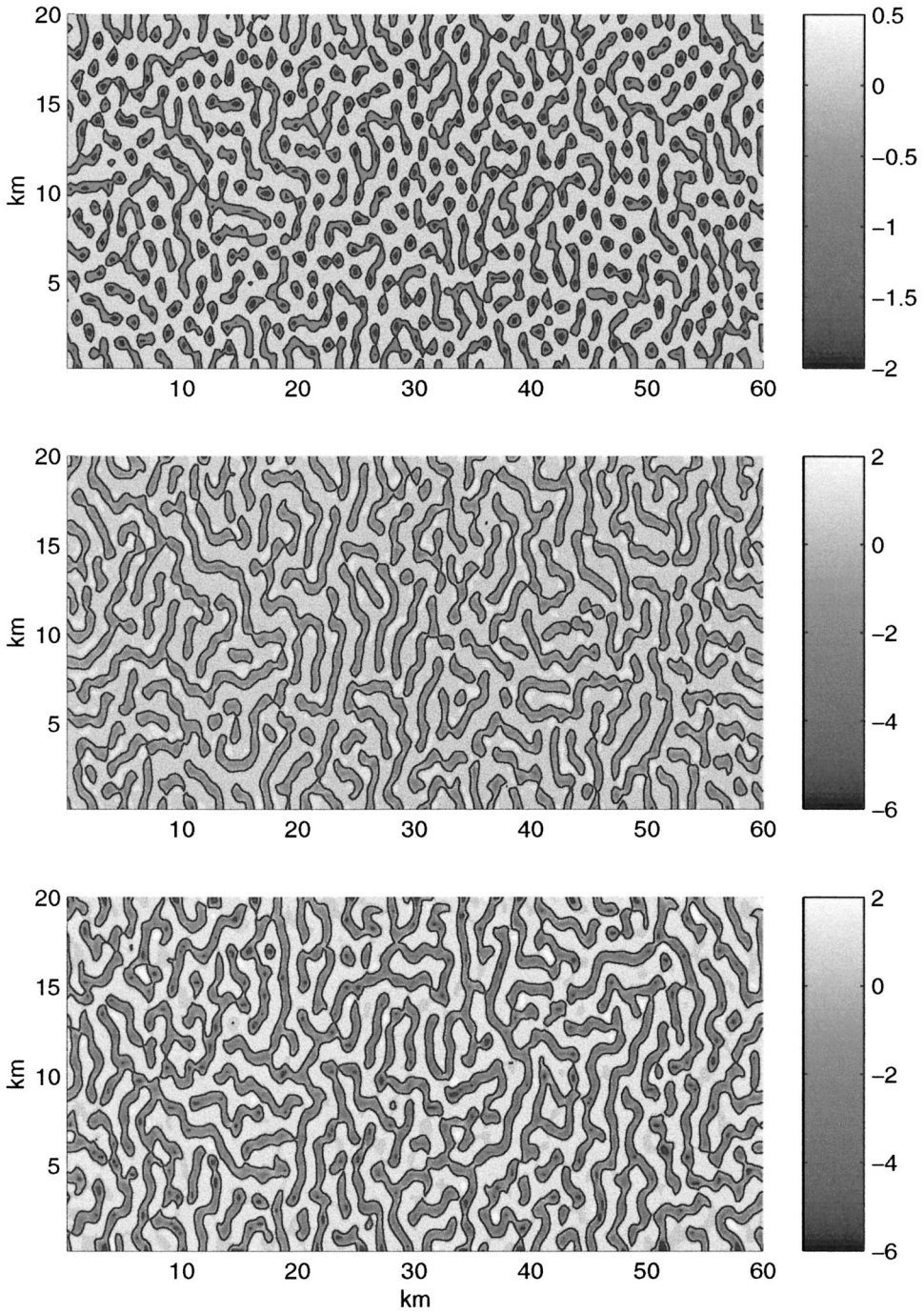

FIG. 4. As in the Fig. 2 but in the case when B has no spatial gradients. Only the vertical velocity (cm s^{-1}) is plotted in grayscale.

These signatures can be readily understood as follows: In the initial stages, the horizontal velocity field responds to the strong convergent velocities of the plumes. The floats therefore converge toward the plumes. At 300 m, these convergences are mainly associated with upward motions during the day 0–1 period because the floats are still located in the lower part of the mixed layer. But after 2 days, the mixed layer is already deeper than 800 m, and the strong convergences at 300 m are now associated with downward motion. The floats at 800 m, however, now in the lower part of the mixed layer, experience strong convergence zones

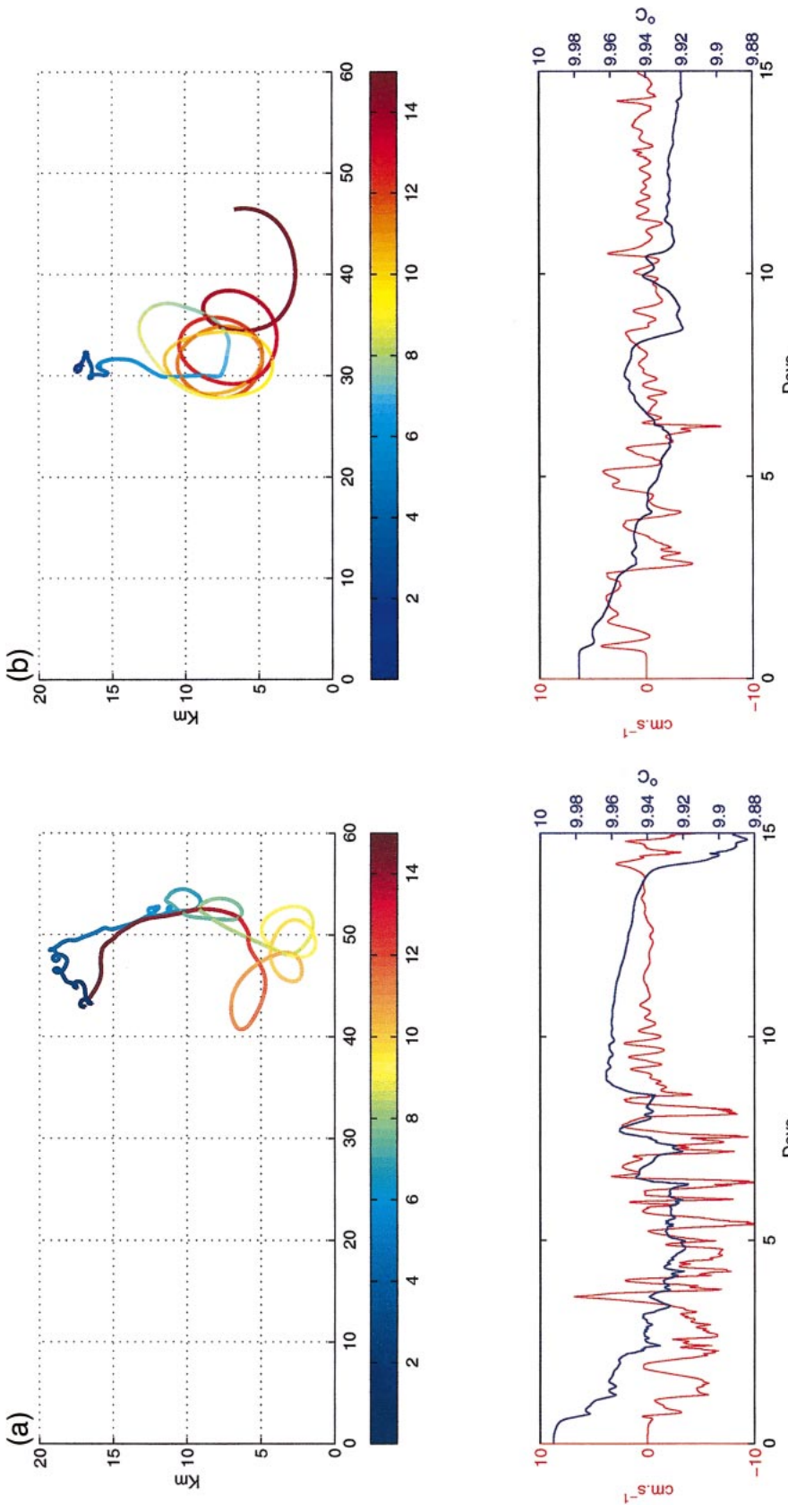

FIG. 5. (top) Trajectory of (a) float at 300 m and (b) float at a depth of 800 m in the experiment with weak stratification (expt 1). Color indicates time in days. (bottom) Red line: vertical velocity (cm s^{-1}) along the float track; blue line: temperature along the float track (°C).

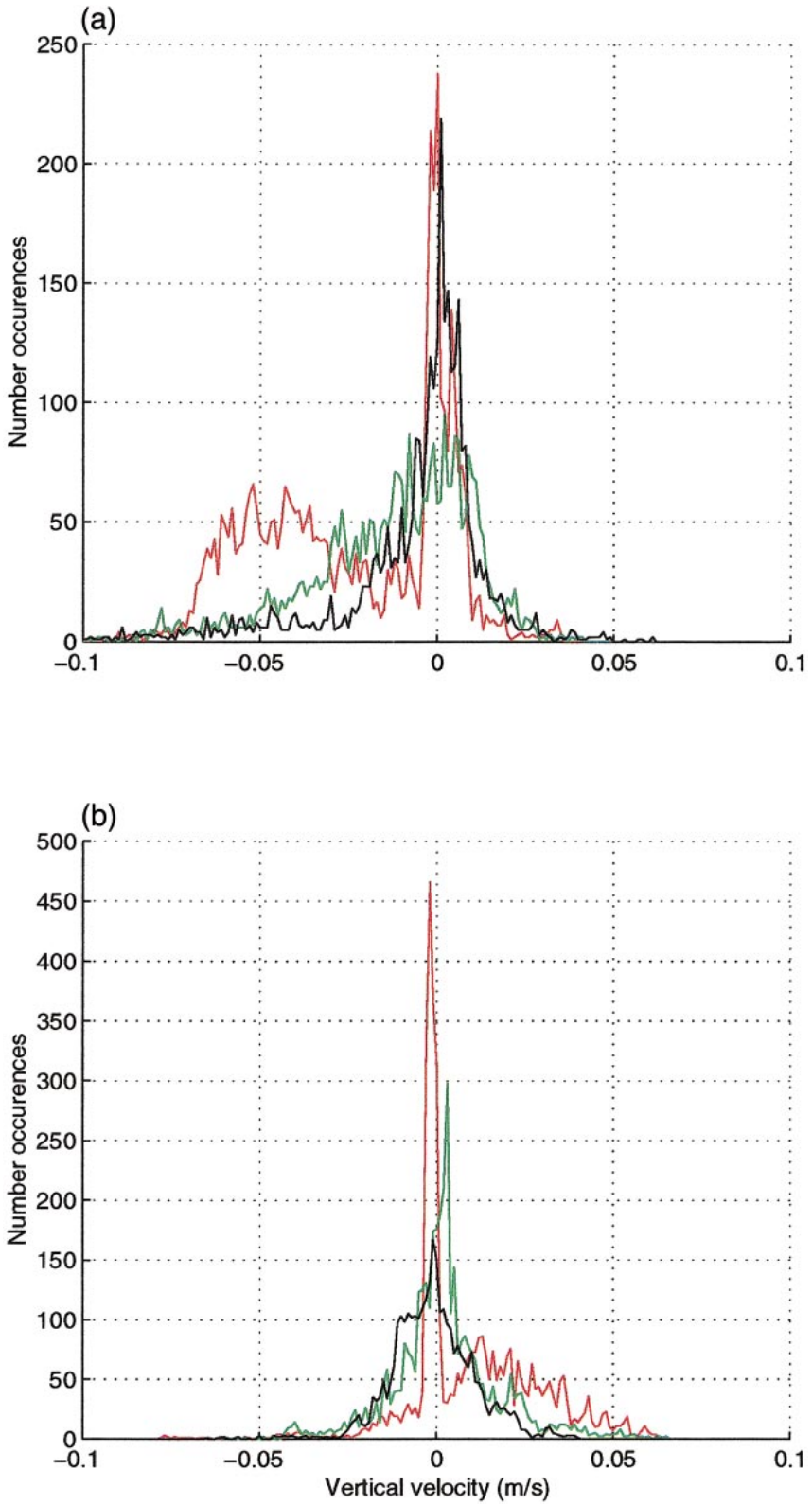

FIG. 6. Probability density function for the vertical velocity of the floats (a) at a depth of 300 m and (b) at a depth of 800 m in expt 1 as a function of time. The occurrences are computed for 1-day periods. Red line: days 2–3; green line: for days 5–6; and the black line is for days 9–10.

associated primarily with upward vertical motion. Hence, we expect the PDF of w to be skewed toward downward motion above and upward below because of the tendency of floats to preferentially sample zones of horizontal convergence (see Lherminier et al. 2001). As time goes on, baroclinic instability develops, and warmer water from the southern part of the channel is advected northward restratifying the column. Convection becomes confined to downwelling fronts, as seen in the bottom panel of Figs. 2 and 3b.

Two processes could account for the observed reduction in the asymmetry of the PDFs of w seen in Figs. 6a and 6b as time proceeds. First, the floats are likely to sample regions with a much wider range of mixed layer depth as time goes on because the floats are swept laterally by eddies to and from regions of very different mixed layer depth. Thus, the negative bias of floats located in deep mixed layers could be canceled by the positive bias measured by them when sampling shallow mixed layer. Second, baroclinic eddies come to dominate the flow as time proceeds (see the progression in Fig. 2). As the eddies spin up, the horizontal area of the fluid occupied by downwelling fronts becomes smaller and is not likely to be well sampled by our Lagrangian floats.

In order to distinguish between these two mechanisms, a second experiment was carried out (expt 2) with 500 floats deployed at 300 m. In this second experiment, a stronger initial stratification was set up with $N_{\text{th}}^2 = 7 \times 10^{-7}\ \text{s}^{-2}$, reducing the rate of deepening of the mixed layer (the atmospheric heat flux is the same as in expt 1). The increased number of floats deployed allows improved sampling for a comparison between Eulerian and Lagrangian statistics. The 2-h mean temperature and vertical velocity (stored every 2 h at 300 m) were averaged over all float trajectories. These were compared to the average of T and w over the basin at 300 m (by definition, the spatial average of w is zero). The 95% confidence interval was computed using the standard deviation of the 2-h mean float data.

As can be seen in Fig. 7a, the mean velocity computed by the floats lies outside the confidence range in the first few days—the w measured by the floats is biased upward. Indeed, because the mesoscale circulation is weak in this initial period, the floats are drawn toward the plumes as described above. In this second integration, because the mixed layer remains rather shallow, the convergence is mainly associated with upward motion, even at 300 m. After 4 days, however, the bias measured by the floats has diminished (and is equivalent to the reduction in the asymmetry of the PDF of w as time proceeds, obtained in the previous experiment). However, if the averages are carried out over those floats located in a mixed layer shallower than 400 m (Fig. 8), the bias persists beyond 4 days, suggesting that the bias is a consequence of the position of the float within the mixed layer. To investigate, the mixed layer depth was diagnosed from the potential vorticity field, as described

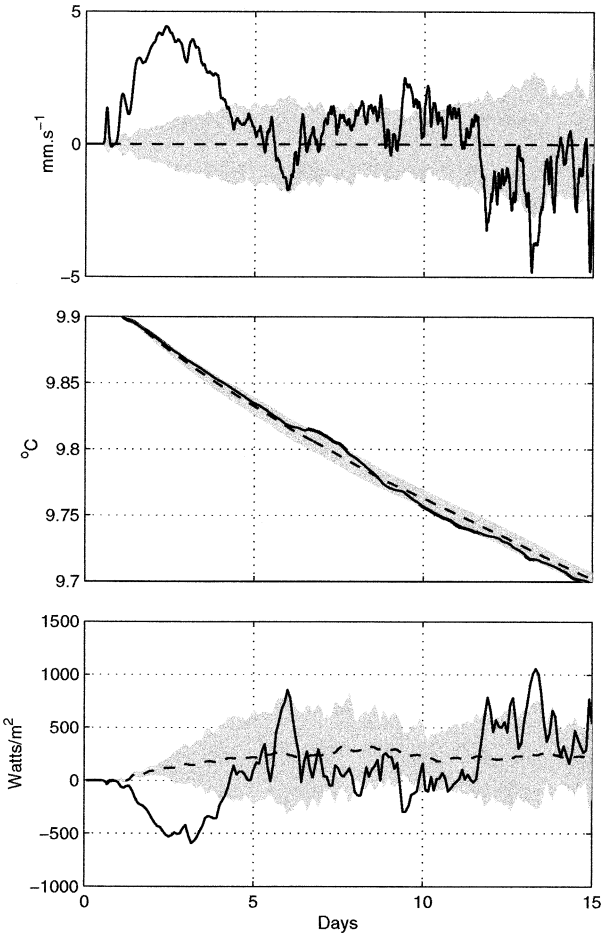

FIG. 7. (top) Vertical velocity averaged over all the float trajectories (solid line) at a depth of 300 m in expt 2. The 95% confidence interval (indicated by the shading) is computed using the formula $\overline{X} \pm 2.78\ \sigma/\sqrt{n}$, where σ is the standard deviation and n is the number of floats. (middle) Temperature averaged over all the float trajectories (solid line), and temperature averaged over all the grid points of the model at 300 m (dotted line). The 95% confidence interval is shaded. (bottom) As in the middle panel but for $\overline{w'T'}$.

in HM (see also legend of Fig. 9), and stored at each float position. The vertical velocity measured by the floats was then plotted as a function of the *relative* position of the float in the mixed layer (i.e., as a function of z/H_{mix}, where z is the depth of the float and H_{mix} is the depth of the mixed layer) for days 0–3, when the mesoscale activity is negligible, and for days 7–10, when the mesoscale activity was fully developed. Figure 9 reveals that for both intervals, the bias in w is positive when the floats are located in the lower part of mixed layer and negative when the floats are situated in the upper part of the mixed layer, irrespective of the presence of geostrophic eddies. The curves in Fig. 9 are similar to those of Lherminier et al. (2001, their Fig. 9), even though the Lherminier et al. calculation did not model geostrophic eddies. We conclude, therefore, that the diminution of the bias in w as time proceeds in Fig.

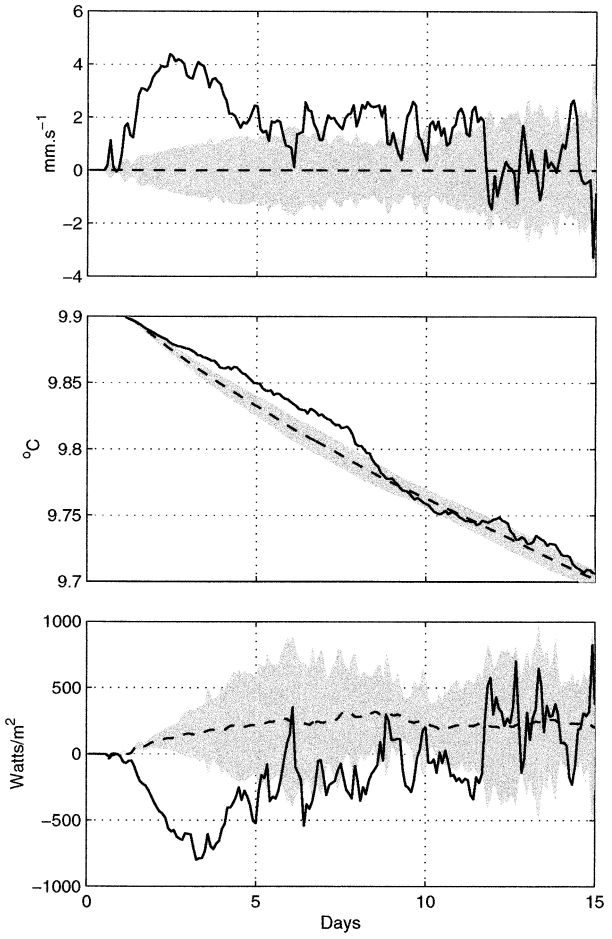

FIG. 8. Same as in Fig. 7, but the averages are carried out for only those floats that located in an area where the mixed layer is shallower than 400 m.

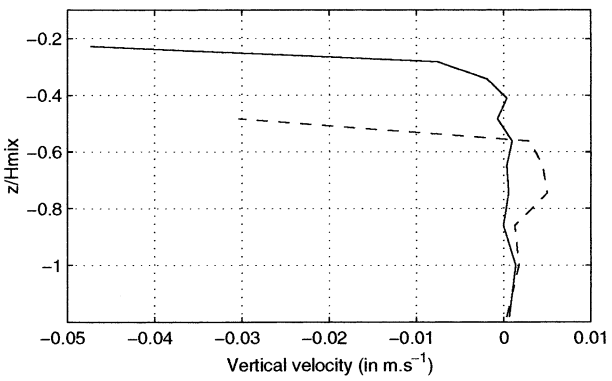

FIG. 9. Mean vertical velocity computed by the floats as a function of z/H_{mix}, where z is the depth at which the float is deployed and H_{mix} is the depth of the mixed layer. The dotted line is for days 0–3; continuous line, days 7–10. The $Q^* = 0.5$ contour is chosen to distinguish between mixed fluid and stratified fluid (where Q^* is the Ertel potential vorticity normalized by its initial value in the resting fluid, as defined in HM).

7a is due in part to the fact that the floats are sampling regions with greatly varying mixed layer depths, and that positive biases cancel the negative ones.

Before going on we note also that Legg and McWilliams (2002) set up an experiment in which a geostrophic eddy field is uniformly cooled. The comparison between the Eulerian mean vertical velocity and the estimation of this value by floats also reveals a strong negative bias for the float data, but one that does not diminish with time as in the experiment described here. Indeed, in their experiment the surface heat loss is uniform, the isobaric floats do not sample widely varying mixed layer depths, and the bias is of one sign. On the contrary in our experiment, shallow mixed layers coexist with deep mixed layers, and the floats are moved by the mesoscale motion from shallow mixed layer regions to deep mixed layer regions.

c. Vertical and lateral buoyancy transport

1) ESTIMATES OF VERTICAL HEAT FLUX FROM FLOATS

In the experiment with strong stratification (expt 2) vertical heat fluxes were estimated from simulated float data. As there were a large number of floats (500), the perturbation of T at a float position was computed from a spatial average (over all the floats) of the temperature at a given time: $T' = T_{\text{float}} - \overline{T}_{\text{all floats}}$. The perturbation of w was computed in the same way. The mean (over all the floats) vertical heat flux deduced from these perturbation fields, $\overline{w'T'}$, is compared in Fig. 7c with the average over the whole basin of the vertical heat flux computed from Eulerian data. The 95% confidence interval is also plotted. As for the vertical velocity, in the first 4 days the float data are biased. The floats located in the northern half of the channel are preferentially trapped in convergence zones associated with upper motions. In these convergence zones the temperature is lower than the ensemble mean temperature of all the floats because (approximately) half of them are located in the warmer southern half of the channel. Thus, in these early stages, the heat flux computed from the floats is negative (downward) even though the applied heat flux is positive. One can also notice that the heat flux evolution follows the evolution of w. As a consequence of the decorrelation between T and w, the vertical heat flux variations are dominated by the variations of w, which present stronger amplitudes with respect to the mean and higher frequencies than the variations of T. As time proceeds, the estimate of vertical heat flux from the floats becomes closer to that deduced from Eulerian calculations.

Attempts to separate the vertical heat flux $\overline{w'T'}$ into a high frequency component and a low frequency component led to ambiguous results. The trend in the temperature time series following floats is difficult to remove, because they depend on individual float trajec-

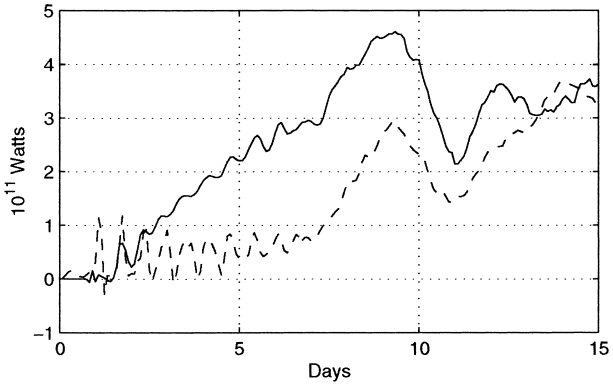

FIG. 10. Meridional heat transport at midchannel (10^{11} W) (dashed line) and vertical heat transport through the total surface of the channel at a depth of 300 m (10^{11} W) (solid line) as a function of time in expt 2. The total flux of heat being taken out of the channel is 4.8 $\times$ 10^{11} W.

tories and vary from float to float. Moreover, a record of 15 days is not long enough to separate between high and low frequencies.

2) EULERIAN MEANS

In Fig. 10 we diagnose the Eulerian lateral and vertical heat flux in the channel as a function of time for experiment 2. The horizontal flux ($\overline{vT}^{xz}$ in watts) is computed at midchannel and is the integral from the bottom to the top and from east to west. The vertical flux ($\overline{wT}^{xy}$ in watts) is the flux through the 300-m surface integrated over the channel. The $\overline{vT}^{xz}$ time series shows that lateral processes are small initially but play a dominant role after 7 days or so. The total flux of heat being taken out of the top of the channel is 4.8 $\times$ 10^{11} W (or 400 W m^{-2} on average), to which the lateral heat flux should be compared. From 7 days onward, horizontal fluxes play a major role in compensating the surface heat flux over the northern half of the basin and keeping it warm and restratifying it (see Fig. 3c). The $\overline{wT}^{xy}$ flux increases more or less linearly during the first 7 days: plumes draw heat vertically to the surface of the channel to compensate surface heat loss. But beyond 7 days the vertical and horizontal fluxes appear to vary together, suggesting that baroclinic instability is also a key player in vertical heat transport in the latter stages of the integration (in HM, it was shown that baroclinic instability was a more important player in the restratification than symmetric instability). We tried to separate the vertical heat fluxes associated with plumes and mesoscale eddies when both coexist. Because the w associated with plumes is an order of magnitude larger than the w associated with mesoscale eddies, it is difficult to clearly separate the mesoscale signal. However, Fig. 10 suggests that both mesoscale and small scales made a comparable contribution to $\overline{w'T'}$.

4. Buoyancy transport across the mixed layer

We saw in section 3 that as the (numerical) fluid evolves from convection to baroclinic instability, the statistical signatures of plumes, as revealed in the skewness of the PDFs of w, become less pronounced in the presence of fully developed large-scale eddies. We now discuss how one might relate the buoyancy transport due to eddies to properties measured by the floats that sample them.

We suppose, guided by previous studies of the transfer properties of baroclinic instability and following HM, that the lateral flux of buoyancy across the channel can be written

$$\overline{v'b'} = -K\overline{b}_y = -KM^2, \tag{2}$$

where $M^2 = |\overline{b}_y|$ is the meridional buoyancy gradient in the mean and K is an eddy transfer coefficient related to mean-flow quantities thus:

$$K = c_e L_{\text{zone}} v_{\text{eddy}}. \tag{3}$$

Here L_{zone} is the transfer length scale [and is set equal to L_f, the scale imposed by the forcing, Eq. (1) (see discussion in HM)], v_{eddy} is a measure of the typical eddy velocity, and c_e is an efficiency factor (see Jones and Marshall 1997).

Motivated by Fig. 10, we hypothesize that, in the presence of a fully developed field of geostrophic eddies, the lateral buoyancy flux across the convective layer of depth h (taken at midchannel) balances the difference in buoyancy loss between the north and the south of the channel thus:

$$h\overline{v'b'} = L_{\text{zone}}\overline{\Delta B}, \tag{4}$$

where $\overline{\Delta B}$ is the difference in the buoyancy loss at the sea surface between the northern half of the channel and the southern half.

Note that Eq. (4) is only strictly true if we assume a steady state. We show in HM that the cumulative heat loss from the surface over, say, the northern half of the channel is initially balanced by deepening of the mixed layer. However, as baroclinic eddies begin to flux heat laterally through the mixed layer, the rate of deepening becomes markedly less than that expected from one-dimensional considerations. In HM we compute a transfer timescale, τ_{transfer}—the time at which the lateral transfer by eddies becomes significant. In the diagnostic tests of (4) presented below, we use model output at this transfer timescale—that is, h is the mixed layer depth at midchannel at $t = \tau_{\text{transfer}}$.

Using Eqs. (2) and (3), assuming that $v_{\text{eddy}} = |u|$, the mean surface zonal flow in thermal wind balance with the lateral buoyancy gradient given by

$$|u| = \frac{M^2 h}{f}, \tag{5}$$

where f is the Coriolis parameter and h is the mixed

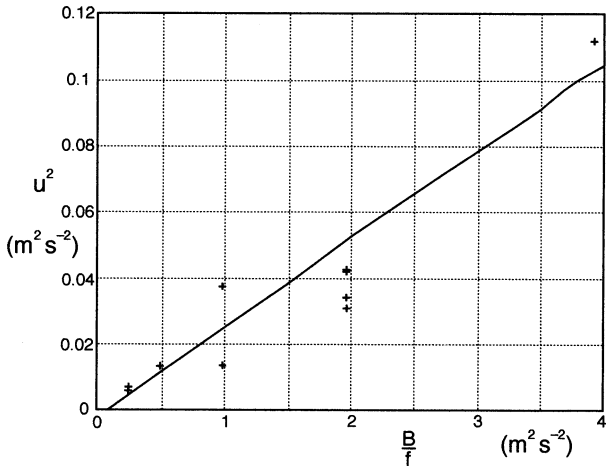

FIG. 11. Horizontal velocity $(u^2 + v^2)^{1/2}$ averaged horizontally and vertically over the mixed layer for each experiment listed in the table, plotted against $B_{1/2}/f$. For the profile of cooling adopted in the experiments [see Eq. (1) with $L_y/L_f = 2$] the difference in the average buoyancy loss between the northern and southern half of the channel required in Eq. (6) is given by $\overline{\Delta B} = 1.33B_{1/2}$.

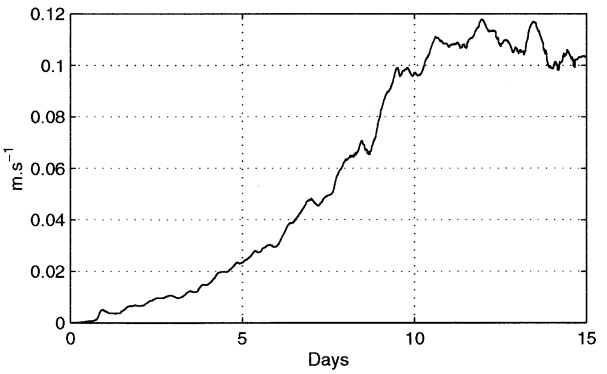

FIG. 12. Horizontal velocity $(u^2 + v^2)^{1/2}$ averaged over all the float trajectories at a depth of 300 m in expt 2.

layer depth at midchannel, the buoyancy balance (4) implies that

$$c_e f v_{\text{eddy}}^2 = \overline{\Delta B}. \tag{6}$$

Thus, the horizontal currents in our channel should scale like

$$v_{\text{eddy}} = \frac{1}{c_e^{1/2}} \left(\frac{\overline{\Delta B}}{f} \right)^{1/2} \tag{7}$$

if the eddies associated with them are important players in the buoyancy budget of the mixed layer, as assumed in Eq. (4).

The horizontal speed, $(u^2 + v^2)^{1/2}$, averaged horizontally and vertically over the mixed layer is plotted for the experiments set out in the table against the prediction, $u_{\text{rot}} = (\overline{\Delta B}/f)^{1/2}$, in Fig. 11. The broad agreement is encouraging, suggesting that the simple ideas set out above have some validity. From the slope of the line we deduce that $c_e = 0.053$ [encouragingly close to, but between the value of 0.04 found in Jones and Marshall (1997) or Spall and Chapman (1998) and the value 0.08 deduced in HM], and so $u \approx 4\ (\overline{\Delta B}/f)^{1/2}$. It is fascinating to note the connection between Eq. (7) and $u_{\text{plume}} \sim (B/f)^{1/2}$, the velocity scale of plumes generated by the uniform cooling of a fluid at rate B in the presence of rotation f (see Jones and Marshall 1993). The horizontal swirl currents associated with the homogeneous field of plumes, shown in Fig. 4, does indeed scale like v_{rot} depending on B rather than $\overline{\Delta B}$. Instead, the mature baroclinic eddies that ultimately dominate when the buoyancy forcing has spatial gradients have a velocity scale (7) that depends on $\overline{\Delta B}$.

In Fig. 12 the average horizontal speed measured by all the floats at a depth of 300 m is plotted as a function of time. We see the increase in speed as the geostrophic eddies build up in strength. Evaluating the ''law of buoyancy transport'' from the float data—using Fig. 12 to obtain v_{eddy}^2 in Eq. (6) and assuming a $c_e = 0.05$—we deduce a lateral heat transport across the channel sufficient to balance a $\overline{\Delta B}$ of $\sim$100 W m^{-2}, a significant fraction of the $\overline{\Delta B}$ of 400 W m^{-2} imposed in the model.

5. Conclusions

The ocean responds to buoyancy loss at its upper surface through the agency of convection and baroclinic instability. Both coexist and each plays a role in the transport of buoyancy through the evolving boundary layer. The interplay was studied here by setting up an initial value problem in which, as time proceeds, convection gives way and coexists with baroclinic instability. In the presence of fully developed geostrophic eddies, intense downwelling becomes confined to frontal regions. Numerous isobaric floats were deployed to obtain good statistics, which are compared with Eulerian data.

We find that, in the initial days of the experiment, the PDFs of w, measured by the floats, exhibit a skewness that depends in a clear and understandable way on the sign and magnitude of the horizontal divergence field, as discussed in Lherminier et al. (2001). The horizontal divergence field (i.e., the w) measured by floats depends on their level in the water column relative to the depth of the convective layer. However, as time proceeds, the skewness computed over all the floats at a given level is reduced. This can be understood in terms of the fact that, as time goes on, the range of variation of the mixed layer depth increases, and the floats undergo positive and negative biases that more or less cancel out. Mesoscale eddies play an indirect role by moving floats from regions of shallow mixed layer to deep mixed layer.

As observed in real float data, the time series of temperature and vertical velocity measured by the simulated floats do not show a high correlation. While w exhibits large downward velocity of a duration of 3–6 h, characteristic of plumelike behavior, temperature is domi-

nated by smaller amplitudes and longer timescales associated with mesoscale activity. Therefore, the variations of the vertical heat flux computed from float data are mainly dominated by the variations of w. Thus, vertical heat flux measured by isobaric floats exhibits similar biases to w. Attempts to separate the vertical heat flux $\overline{w'T'}$ into a high frequency component and a low frequency component led to ambiguous results. We also tried to separate low-frequency and high frequency signals using Eulerian data at a fixed level. In this case it was possible to associate high temporal frequencies with small spatial scales and low frequencies with large spatial scales, but, even with Eulerian data, it is difficult to clearly separate the mesoscale signal. However, over the period of the record, it appeared that both mesoscale and small scales made a comparable contribution to $\overline{w'T'}$.

As an alternative signature of the mechanism of buoyancy transport due to baroclinic eddies, in section 4 we attempted to relate lateral buoyancy transport through the mixed layer to the horizontal velocity variance measured by isobaric floats. This indeed provides a rationalization of lateral buoyancy transport in the numerical experiments. It would be interesting to apply and test out the approach to the floats deployed in the Labrador Sea Deep Convection Experiment described in Lavender et al. (2002).

Acknowledgments. We would like to thank the Office of Naval Research, whose support made this work possible. We also acknowledge the comments of two helpful reviewers.

REFERENCES

Garwood, R., R. Harcourt, and P. Lherminier, 2001: Excitation of internal waves by deep convection. *J. Phys. Oceanogr.*, submitted.

Gascard, J. C., and R. A. Clarke, 1983: The formation of Labrador Sea Water. Part II: Mesoscale and smaller-scale processes. *J. Phys. Oceanogr.,* **13,** 1780–1797.

Haine, T. W. N., and J. Marshall, 1998: Gravitational, symmetric, and baroclinic instability of the ocean mixed layer. *J. Phys. Oceanogr.,* **28,** 634–658.

Jones, H., and J. Marshall, 1993: Convection with rotation in a neutral ocean: A study of open-ocean convection. *J. Phys. Oceanogr.,* **23,** 1009–1039.

——, and ——, 1997: Restratification after deep convection. *J. Phys. Oceanogr.,* **27,** 2276–2287.

Lab Sea Group (J. Marshall, F. Dobson, K. Moore, P. Rhines, M. Visbeck, E. d'Asaro, K. Bumke, S. Chang, R. Davis, K. Fisher, R. Garwood, P. Guest, R. Harcourt, C. Herbaut, T. Holt, J. Lazier, S. Legg, J. McWilliams, R. Pickart, M. Prater, I. Renfrew, F. Schott, U. Send, W. Smethie), 1998: The Labrador Sea Deep Convection Experiment. *Bull. Amer. Meteor. Soc.,* **79,** 2033–2058.

Lavender, K. L., R. E. Davis, and W. B. Owens, 2002: Observations of open-ocean deep convection in the Labrador Sea from subsurface floats. *J. Phys. Oceanogr.,* **32,** 511–526.

Legg, S., and J. McWilliams, 2000: Temperature and salinity variability in heterogeneous oceanic convection. *J. Phys. Oceanogr.,* **30,** 1188–1206.

——, and ——, 2002: Sampling characteristics from isobaric floats in a convective eddy field. *J. Phys. Oceanogr.,* **32,** 527–544.

——, ——, and J. Gao, 1998: Localization of deep ocean convection by a mesoscale eddy. *J. Phys. Oceanogr.,* **28,** 944–970.

Lherminier, P., R. R. Harcourt, R. W. Garwood, and J. C. Gascard, 2001: Interpretation of mean vertical velocity measured by isobaric floats during deep convective events. *J. Mar. Syst.,* **29,** 221–237.

Marshall, J., and F. Schott, 1999: Open-ocean convection: Observations, theory and models. *Rev. Geophys.,* **37,** 1–64.

——, A. Adcroft, C. Hill, L. Perelman, and C. Heisey, 1997a: A finite-volume, incompressible Navier–Stokes model for studies of the ocean on parallel computers. *J. Geophys. Res.,* **102** (C3), 5753–5766.

——, C. Hill, L. Perelman, and A. Adcroft, 1997b: Hydrostatic, quasi-hydrostatic and non-hydrostatic ocean modelling. *J. Geophys. Res.,* **102** (C3), 5733–5752.

Spall, M. A., and D. C. Chapman, 1998: On the efficiency of baroclinic eddy heat transport across narrow fronts. *J. Phys. Oceanogr.,* **28,** 2275–2287.

Stommel, H., A. D. Voorhis, and D. C. Webb, 1971: Submarine clouds in the deep ocean. *Amer. Sci.,* **59,** 716–722.